Covalent linkage of sulfated hyaluronan to the collagen scaffold Mucograft® enhances scaffold stability and reduces proinflammatory macrophage activation *in vivo*

Sarah Al-Maawi [a,1], Sandra Rother [b,d,1], Norbert Halfter [b], Karen M. Fiebig [b], Juliane Moritz [b], Stephanie Moeller [c], Matthias Schnabelrauch [c], Charles James Kirkpatrick [a], Robert Sader [a], Hans-Peter Wiesmann [b], Dieter Scharnweber [b], Vera Hintze [b,**], Shahram Ghanaati [a,*]

[a] *Clinic for Maxillofacial and Plastic Surgery, Goethe University, Frankfurt Am Main, Germany*
[b] *Institute of Materials Science, Max Bergmann Center of Biomaterials, TU Dresden, Budapester Str. 27, 01069, Dresden, Germany*
[c] *Biomaterials Department, INNOVENT e.V., Prüssingstr. 27B, 07745, Jena, Germany*
[d] *Department of Cellular and Molecular Medicine, Glycobiology Research and Training Center, University of California, San Diego, La Jolla, CA, USA*

ARTICLE INFO

ABSTRACT

Sulfated glycosaminoglycans (sGAG) show interaction with biological mediator proteins. Although collagen-based biomaterials are widely used in clinics, their combination with high-sulfated hyaluronan (sHA3) is unexplored. This study aims to functionalize a collagen-based scaffold (Mucograft®) with sHA3 via electrostatic (sHA3/PBS) or covalent binding to collagen fibrils (sHA3+EDC/NHS). Crosslinking without sHA3 was used as a control (EDC/NHS Ctrl). The properties of the sHA3-functionalized materials were characterized. *In vitro* growth factor and cytokine release after culturing with liquid platelet-rich fibrin was performed by means of ELISA. The cellular reaction to the biomaterials was analyzed in a subcutaneous rat model. The study revealed that covalent linking of sHA3 to collagen allowed only a marginal release of sHA3 over 28 days in contrast to electrostatically bound sHA3. sHA3+EDC/NHS scaffolds showed reduced vascular endothelial growth factor (VEGF), transforming growth factor beta 1 (TGF-β1) and enhanced interleukin-8 (IL-8) and epithelial growth factor (EGF) release *in vitro* compared to the other scaffolds. Both sHA3/PBS and EDC/NHS Ctrl scaffolds showed a high proinflammatory reaction (M1: CD-68+/CCR7+) and induced multinucleated giant cell (MNGC) formation *in vivo*. Only sHA3+EDC/NHS scaffolds reduced the proinflammatory macrophage M1 response and did not induce MNGC formation during the 30 days. SHA3+EDC/NHS scaffolds had a stable structure *in vivo* and showed sufficient integration into the implantation region after 30 days, whereas EDC/NHS Ctrl scaffolds underwent marked disintegration and lost their initial structure. In summary, functionalized collagen (sHA3+EDC/NHS) modulates the inflammatory response and is a promising biomaterial as a stable scaffold for full-thickness skin regeneration in the future.

1. Introduction

Collagen-based biomaterials are frequently utilized in different medical indication fields, especially in terms of tissue engineering [1,2]. Additionally, collagen-based materials are used as wound dressings to support wound healing in critical size wounds and to avoid autologous skin transplantation [3].

Collagen is a ubiquitous protein in the extracellular matrix (ECM) that exhibits different beneficial properties to facilitate the regeneration process [4]. It serves as a scaffold for regenerative cells, and its natural source and interindividual biocompatibility make it a favorable material for clinical application [5]. However, during processing and purification

of naturally derived biomaterials, different protocols, including physical and chemical methods, may affect its natural structure and lead to a foreign body reaction *in vivo* [6,7].

After biomaterial application *in vivo*, the initial wound healing process modulates the biomaterial-induced cellular reaction [8]. Some studies have shown that the biomaterial surface properties predefine the induced cellular reaction [8,9]. Xenogeneic collagen-based materials gained from identical species, e.g., porcine, can induce different *in vivo* cellular reactions dependent on to their physicochemical characteristics, such as pore size, thickness, surface hydrophilicity and surface roughness, and the processing methods they undergo [10,11]. The implantation of a non-crosslinked collagen membrane gained from porcine donors in a subcutaneous mouse model showed a mild cellular reaction including only mononuclear cells (MNCs), which are critical for the physiological wound healing (for example monocytes, macrophages and lymphocytes) [12]. Consequently, the material preserved its initial structure over the observation time of 60 days and did not show early degradation [12]. Using the same implantation model, further studies showed different patterns of cellular reactions for many different collagen-based biomaterials, that are extracted from the same species, i. e., porcine. In this case, the materials induced, in addition to MNCs that are part of the wound healing process, multinucleated giant cells (MNGCs) [6]. Consequently, on day 60 after implantation, the materials lost their initial structure and underwent premature degradation and fibrous tissue influx. Studies have reported that the formation of biomaterial-induced MNGCs takes place after the accumulation and fusion of macrophages during a chronic inflammation process [6]. Similarly, these cells were observed in diseases such as tuberculosis [13]. However, the function of biomaterial-induced MNGCs in the implantation bed is not yet completely elucidated [14]. These studies highlight the role of the physicochemical properties of the materials and the material origin for the induced cellular reaction and inflammatory pattern.

Various modification techniques have been introduced to promote the regenerative potential of collagen-based biomaterials, such as surface modification and crosslinking [15]. However, changing the physicochemical properties of biomaterials directly influences cellular reactions, especially with respect to macrophages [16]. For example, chemical crosslinking of collagen-based materials that should improve the mechanical stability of the materials resulted in a strong inflammatory reaction [17]. As main players in the wound healing process, macrophages have different phenotypes and can express either proinflammatory (M1) [18] or anti-inflammatory (M2) molecules [19]. During regeneration, the polarization of macrophages towards these phenotypes may change according to the inflammatory pattern of their microenvironment [20]. In particular, the biomaterial surface and interaction with the immune system have a great influence on macrophage polarization and thereby the course of the regeneration process.

In addition to collagen, glycosaminoglycans (GAGs) including hyaluronan (HA), are important multifunctional substances in the skin ECM [21]. Collagen consists not only of peptide sequences required for cell adhesion but also positively charged binding sites for GAGs [22]. This property can be utilized to noncovalently bind negatively charged molecules, such as sulfated hyaluronan (sHA3) derivatives, within a collagen network [23]. A further approach to tether GAG derivatives to protein-based scaffolds is covalent amine coupling, which also results in the crosslinking of collagen [24]. In particular, sHA3, which contains 3 sulfate groups per disaccharide unit, demonstrated promising potential to functionalize biomaterials since it promotes the proliferation of fibroblasts and endothelial cells [25,26]. Furthermore, sHA3 has immunomodulatory properties and shows a strong interaction with several biological mediator proteins, such as the growth factors and cytokines involved in dermal wound healing [27–29]. The aim of the present study was to evaluate the hypothesis that the inflammatory response of collagen-based scaffolds may be modified by sHA3. In this context, this study analyzes the regenerative capacity of collagen-based scaffolds

modified by surface functionalization using negatively charged sHA3. Three different modifications per collagen-based scaffold were characterized and evaluated *in vitro* and *in vivo* to elucidate the influence of sHA3 and crosslinking via EDC/NHS on the cellular inflammatory reaction, vascularization and degradation patterns of the biomaterials.

2. Material and methods

2.1. Materials

A collagen matrix commonly used clinically as a scaffold (Mucograft®) was purchased from Geistlich (Baden-Baden, Germany). The collagen matrix is composed of non-cross-linked collagen type I and III. High-sulfated hyaluronan (sHA3) was synthesized and characterized as described previously [30]. On average, sHA3 contained 3.0 sulfate groups per disaccharide unit (D.U.) as determined by elemental analysis. Further, gel permeation chromatography and laser light scattering detection revealed a weight-average molecular weight of 62 kDa.

Human recombinant epidermal growth factor (EGF) was purchased from MACS Miltenyi Biotec (Bergisch Gladbach, Germany). Reagents were supplied by Sigma-Aldrich (Schnelldorf, Germany) if not noted otherwise.

2.2. Scaffold modification and characterization

2.2.1. Functionalization of collagen-based scaffolds with sulfated hyaluronan

Collagen-based scaffolds (2 × 3 cm in case of Mucograft®) were incubated with 2.5 mM D.U. sHA3 dissolved in phosphate-buffered saline (pH 7.4) (PBS) to allow the noncovalent association of sHA3 with positively charged regions of the collagen fibrils. For the covalent linkage of sHA3 to collagen, scaffolds were treated for 240 min with 2.5 mM D.U. sHA3 was dissolved in 50 mM 2-(*N*-morpholino)ethane sulfonic acid (MES) buffer (pH 5.5) including 0.1 M *N*-(3-dimethylaminopropyl)-*N*′-ethylcarbodiimide (EDC) and 0.05 M *N*-hydroxysuccinimide (NHS) to activate the carboxylic acid groups of sHA3. Samples that were treated in a similar way with 50 mM MES buffer (pH 5.5) comprising 0.1 M EDC and 0.05 M NHS without sHA3 served as crosslinked controls. Afterwards, the samples were lyophilized. The freeze-dried scaffolds were washed twice with water for 120 s, transferred into new well plates and freeze-dried again (Fig. 1 A).

Sterile samples for use in *in vivo* experiments were obtained by using sterile filtrated solutions and by conducting each scaffold functionalization step under sterile conditions. For *in vitro* and animal experiments, scaffolds with a diameter of 6 mm were prepared using disposable biopsy punches (Pfm medical, Cologne, Germany).

2.2.2. Scaffold characterization

The functionalized scaffolds were incubated in PBS for up to 28 days to examine their stability and sHA3 release profiles. The amounts of sHA3 within the scaffolds were quantified after complete collagen degradation via papain (1 mg/ml in PBS) at 60 °C using the cationic dye dimethylmethylene blue (DMMB) according to a previous study [31]. Defined concentrations of sHA3 dissolved in PBS were used for calibration. The distribution of sHA3 inside the functionalized scaffolds was visualized using Toluidine Blue staining as described before [24]. In brief, scaffolds were incubated in 1 ml of Toluidine Blue solution (0.05 mg/ml in 10 mM hydrochloric acid) for 10 min and destained with deionized water till the sHA3-free control samples were decolorized completely. Afterwards the hydrogels were cut in halves and freeze-dried. The amount of released collagen was determined via Lowry assay [32] with collagen type I as the protein standard.

The number of free ε-amino groups within the collagen scaffolds was determined after reaction with 2,4,6-trinitrobenzenesulfonic acid as described by Wang et al. [33] with modifications according to another previous study [34]. The crosslinking degree was calculated by
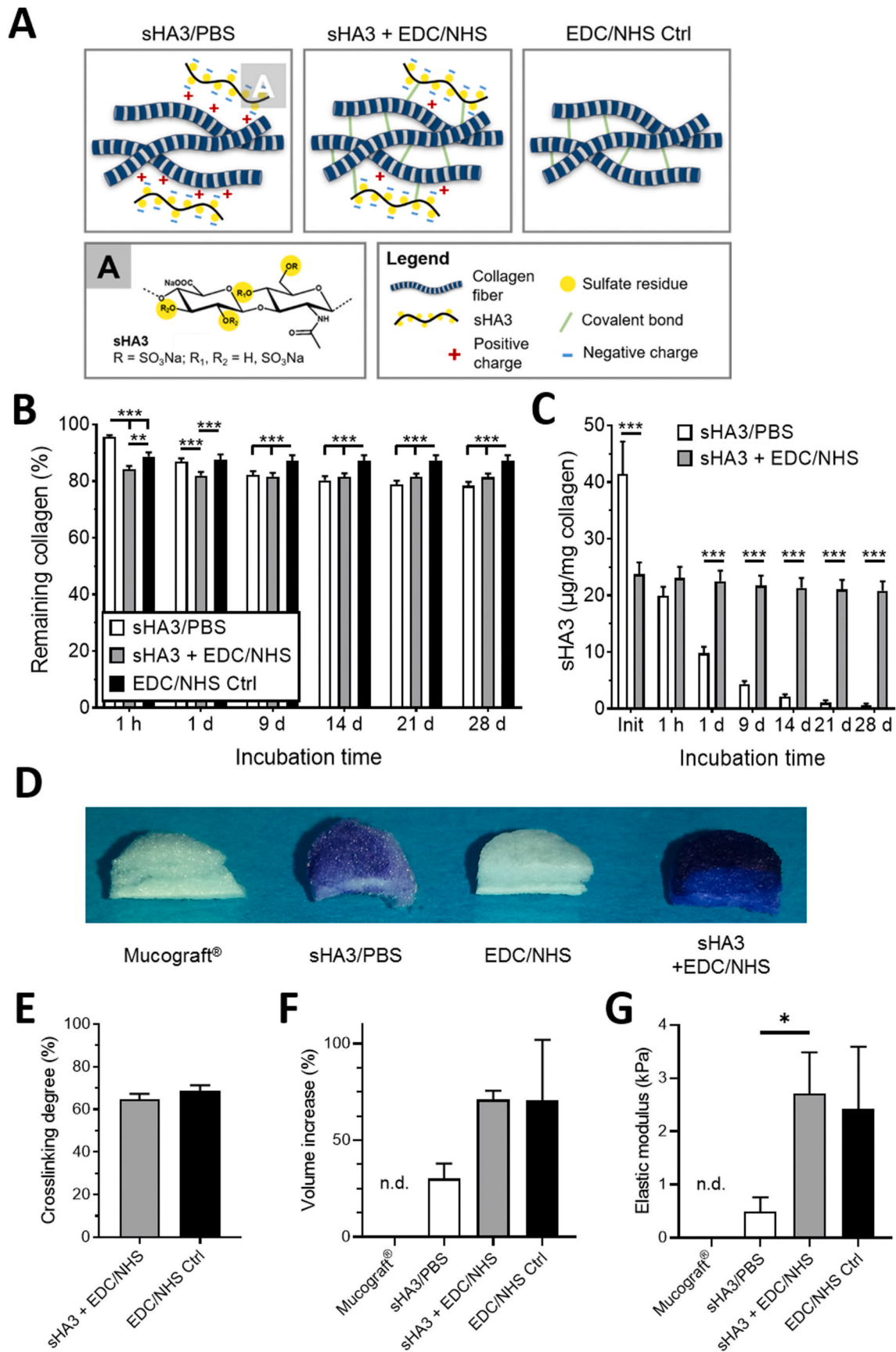
(caption on next page)

Fig. 1. Functionalization and characterization of collagen-based scaffolds A) Schematic of scaffold functionalization with sHA3. Upper panel from left to right: Negatively charged residues of sHA3 interact with positively charged regions within the collagen fibers, leading to collagen-based scaffolds with physically bound sHA3 (sHA3/PBS). Carboxylic groups of sHA3 present within the collagen fibers react with ε-amino groups of collagen after activation with EDC/NHS. This reaction results in crosslinked collagen scaffolds with covalently bound sHA3 (sHA3 + EDC/NHS). Collagen scaffolds incubated with EDC/NHS in the absence of sHA3 served as crosslinked controls (EDC/NHS Ctrl). Lower panel: Structure of the repeating disaccharide unit of sHA3. B) The remaining amounts of collagen after collagen matrix treatments with sHA3 and/or EDC/NHS were indirectly determined by measuring the amount of protein in the supernatants via the Lowry method after incubation in PBS at 37 °C. The amounts of incorporated sHA3 after collagen matrix (C) functionalization and incubation in PBS at 37 °C were quantified via the DMMB assay. Distribution of sHA3 within the hydrogels was determined via the Toluidine Blue assay. After staining the hydrogels were cut into halves and freeze-dried (D). The amount of free ε-amino groups before and after incubation of the collagen-based materials was used to calculate the crosslinking degree of collagen (E). Modified scaffolds were swollen at room temperature in PBS for 2 h and volume increase was determined (F). The elastic modulus was determined after swelling in PBS at room temperature (G). Volume increase and elastic modulus was not determined (n.d.) for Mucocraft® due to its low stability in PBS. Two-way ANOVA: (**) $p < 0.01$ and (***) $p < 0.001$. (For interpretation of the references to color in this figure legend, the reader is referred to the Web version of this article.)

subtracting the quotient of the absorption of the crosslinked and the non-crosslinked collagen samples with respect to one. The volume increase (VI) of the scaffolds when rehydrated was determined after incubation of 3 mm cylindrical punches of the scaffolds in PBS for 2 h with a digital measuring slide using the following formula: IV [%] = $(V_{HG}-V_{SC})/V_{SC} \times 100\%$ with V_{HG} being the volume of the hydrogel and V_{SC} being the volume of the scaffold. Furthermore, the elastic modulus of the hydrogels was characterized using a CellScale MicroTester (Waterloo, Canada). For determination, 3 mm cylindrical scaffold punches were incubated in PBS for 2 h and measured with 5 μm/s within a maximum strain of about 15%. The slope of the linear graph was used to determine the elastic modulus.

The experiments for scaffold characterization were performed at least in triplicate.

2.2.3. Scanning electron microscopy (SEM)

The freeze-dried samples were mounted onto a sample holder containing carbon tape. Then, the samples were sputtered with a thin carbon layer. A scanning electron microscope (Philips ESEM XL 30, FEI) with a back-scattered electron detector was used to examine the scaffold morphology.

2.3. In vitro study

Liquid platelet-rich fibrin (PRF) is a cell suspension including blood cells such as platelets, leukocytes and their subgroups. This was applied to examine the matrix permeability to fibrin and cells. Moreover, the ability of the scaffold surfaces on the cells in PRF to release different growth factors and cytokines was evaluated [35]. The application of PRF in this study was conducted following the principle of informed consent as approved by the responsible Ethics Commission of the state of Hessen, Germany (265/17).

2.3.1. PRF preparation

Three healthy donors not taking systemic medication were included as blood donors after signing an informed consent document. From each donor, two tubes (20 ml) were withdrawn from the antecubital vein by means of a 24-gauge butterfly needle and i-PRF tubes (Process for PRF, Nice, France). Centrifugation was performed using a tabletop centrifuge (Duo centrifuge, Process for PRF, Nice, France; Mectron, Cologne, Germany, radius: 110 mm). The blood was centrifuged at 600 rpm (44×g) for 8 min [36]. After the centrifugation process, the blood formed two phases: the lower phase includes mainly red blood cells and the upper phase includes the liquid PRF. The liquid PRF, including platelets, lymphocytes and leukocytes [35] was withdrawn and homogenized prior to its application on the biomaterial.

2.3.2. Biomaterial incubation in vitro

Punches of the functionalized collagen-based scaffolds (6 mm diameter) were used for this procedure. The biomaterials were placed under sterile conditions in 48-well plates with the spongy layer facing upwards (CELLSTAR®, Greiner bio-one). Liquid PRF (300 μl) was added to the scaffolds and cultivated at 37 °C for 1 h until clotting. After

clotting, the scaffolds were covered with 400 μl of the "Roswell Park Memorial Institute" (RPMI) medium with 1% penicillin/streptomycin and cultivated for 3 days. The supernatant was collected, aliquoted and saved at −80 °C until use. The experiments were performed in triplicate. The explants were fixed using Histofix (Roti-Histofix 4% acid free pH 7, Carl-Roth, Germany) for 24 h and analyzed histologically.

2.3.3. Enzyme-linked immunosorbent assay (ELISA)

The supernatants collected after biomaterial incubation with PRF (section 2.3.2) were used to measure the concentrations of vascular endothelial growth factor (VEGF), epidermal growth factor (EGF) transforming growth factor beta-1 (TGF-β) and interleukin 8 (IL-8). ELISA kits (Quantikine® ELISA, R&D Systems, Minneapolis, USA) were used according to the manufacturer's protocols and measured by a microplate reader (Infinite® M200, Tecan, Grödig, Austria). The measurements were performed using a wavelength of 450 nm and a reference reading at 570 nm.

2.4. Animal experimental design and surgery

The design, analyses and reporting of this experiment were performed following the ARRIVE guideline checklist for reporting animal research [37]. All the animals participating in this experiment were part of an approved project by the animal care facility ([ZFE] Frankfurt am Main, Germany) from the Department of Medicine of the Johann Wolfgang Goethe University Frankfurt and the regional council committee (Project No. FK/1023; Darmstadt, Germany) according to German law. During the study time, animals were kept under controlled environment (20 °C, light/dark cycles of 12 h and humidity of 40%–70%, regular rodent pellets and water *ad libitum*). Surgery was performed after 1 week of acclimatization period at the animal facility.

2.4.1. Subcutaneous biomaterial implantation

In total, sixty (n = 4 rats per group (5) per time point (3) = 60 rats) female Wistar rats (*Rattus norvegicus*, 6–8 weeks) were obtained from Charles River (Sulzfeld, Germany). Anesthesia was induced with a combination of ketamine (50 mg/kg) and xylazine (5 mg/kg), that was injected intraperitoneally. After anesthesia, the animal's subscapular region was shaved and sterilized using antiseptic solution (Octeniderm®, Bonn, Germany). All biomaterials were prepared in punches 6 mm in diameter. Briefly, an incision was performed at the skin of the rostral portion of the interscapular region. Subsequently, the subcutaneous pocket was prepared within the tissue under the skin muscle as previously described [40,41]. The animals received the differently

Table 1
Animal number and distribution.

Group	Material	Animals per group	Time points
1	Ctrl	4	3, 15, 30 days
2	sHA3/PBS	4	
3	sHA3+EDC/PBS	4	
4	EDC/NHS Ctrl	4	
5	Sham OP	4	

modified scaffolds (Table 1). Subsequently, the subcutaneous pockets were sutured using 5.0 Prolene (Ethicon, NJ, USA). After surgery care included daily health check, oral supplement of tramadol (1–3 mg/kg per day) for pain reduction during the first 3 days after surgery.

2.4.2. Tissue preparation and histology

The tissue samples were fixed in 4% buffered formalin (*Roti-Histofix* 4% acid free pH 7, Carl-Roth, Germany) for 24 h. Next, the explants were cut into five equal sections, placed in histological cassettes, processed by dehydration using a tissue processor (Leica TP1020) and embedded in paraffin blocks. A slide of each segment was cut and stained with hematoxylin and eosin (H&E) for the general histological screening of the implantation bed. Based on the first evaluation, the segment with the best cross-section was selected for each animal for further preparation and staining. Six further consecutive slides with a thickness of 2–3 μm per block per group were cut by means of a rotary microtome (Leica RM 2255, Wetzlar, Germany). Immunocytochemical staining was performed to detect macrophages using a pan marker (CD-68) and to determine their polarization into M1 (CCR-7) and M2 (CD-206); TRAP staining was performed for the detection of tartrate-resistant acid phosphatase activity and von Willebrand factor (VWF) for evaluating vascularization. After deparaffinization and rehydration, the antigen was retrieved using the heat-induced epitope retrieval (HIER) method with citrate buffer with a pH of 6 at 95 °C for 20 min. The samples were rinsed with a buffer solution (Tris buffered saline with Tween 20:1) before staining with monoclonal mouse anti-rat CD-68 (Dako, M0823; concentration 1:800), mouse anti-rat CCR7 (ab32527, concentration: 1:1000, Abcam, UK) mouse anti-rat CD-206 (ab64693, concentration 1:1000, Abcam, UK) and rabbit anti-rat von Willebrand factor (VWF), (ab6994; concentration 1:800; Abcam, UK), matrix metallopeptidase 9 (MMP-9), (Ab58803, concentration 1:250; Abcam, UK) via Autostainer (Lab Vision Autostainer 360, Thermo Fisher Scientific). An anti-mouse secondary antibody was used (HRP Ultravision Quanto Detection System, Thermo Fisher Scientific), and chromogenic visualization was obtained using AEC peroxidase (Dako). Finally, the slides were counterstained with Mayer's hematoxylin. The samples of the *in vitro* experiments were analyzed histologically using conventional hematoxylin and eosin (H&E) staining, and immunohistochemical staining for the antibodies CD-61 (ab225742, concentration 1:2000, Abcam, UK) and CD-45 (ab10558, concentration 1:50, Abcam, UK) using the same protocol described above.

2.4.3. Histological and histomorphometric evaluation of the inflammatory response

Histological and histomorphometric analyses were performed using a light microscope and the slides stained as described in section 2.4.2. The total area of the stained slides was scanned using the "total scan" tool from NIS-Elements software (Nikon, Tokyo, Japan) via a DS-Fi1 digital camera with an Eclipse 80i histological microscope (Nikon, Tokyo, Japan) and an automatic scanning table (Prior Scientific, Rockland, MA). The total scan results in a large image of the whole sample at high resolution (x200 magnification) and allows objective analysis of the total sample. NIS-Elements software was used to perform histomorphometry. For this purpose, the cells were counted using the "annotations and measurements" tool. The cell density of positively stained macrophages and their polarized subtypes (M1/M2) were determined within the biomaterial and the implantation bed after 3, 15 and 30 days of implantation. Manual count of the cells was performed and the number of cells per square millimeter was calculated from the total area of the implantation bed divided by the total number of cells [cells/mm^2]. Similarly, the total numbers of multinucleated giant cells (CD-68 positive) and positively stained cells for CCR-7, MMP-9 or CD-206 were counted manually in the total region of interest and are expressed as the cell density [cells/mm^2]. The biomaterial thickness was measured in the histological cross-section at 50 different points in each sample. The mean of the measurement was considered the biomaterial thickness for each slide.

2.4.4. Statistical analyses

The experiments for scaffold characterization and *in vitro* cultivation were performed at least in triplicate. For the *in vitro* and *in vivo* experiments, statistical analyses were conducted using the collected data displayed as the mean ± the standard deviation. One-way analysis of variance (ANOVA) was used to analyze the quantitative data of the *in vitro* experiments and two-way ANOVA for *in vivo* experiments using Tukey's test with GraphPad Prism (version 7, GraphPad Software, La Jolla, USA). Intraindividual (•) and interindividual (*) significant differences were reported as significant (•; /*) at p values < 0.05 and as highly significant (••/**) at p values < 0.01 and (… /***) at p values < 0.001.

3. Results

3.1. Characterization of sHA3-functionalized scaffolds

Collagen-based scaffolds were functionalized with sHA3, as shown in Fig. 1. After 1 h in buffer, the non-cross-linked samples contained the highest amounts of collagen, while at later time points, the amounts of remaining collagen were almost comparable between the collagen matrices treated with sHA3/PBS and sHA3 + EDC/NHS. However, stability analyses of the collagen-based material treated with EDC/NHS alone (EDC/NHS Ctrl) showed significantly higher amounts of remaining collagen after 9–28 days of incubation in buffer than that in samples incubated with sHA3 in the absence or presence of EDC/NHS (sHA3/PBS, sHA3+EDC/NHS; Fig. 1 B). After treatment with sHA3 in the absence or presence of EDC/NHS, the collagen matrices contained approximately 4 wt% or 2.5 wt% sHA3, respectively (Fig. 1 C). The latter remained quite stable over time, while matrices with physically bound sHA3 (sHA3/PBS) released almost 90% of the initially bound sHA3 within nine days of incubation. It is of note that there was no significant difference regarding the crosslinking degree between EDC/NHS treated samples (Fig. 1 E).

Toluidine Blue staining indicates that sHA3 is well distributed within the spongy layer, while the compact layer was stained to a lesser extent. Scaffolds with physically bound sHA3 (sHA3/PBS) displayed a lighter color in comparison to the EDC/NHS bound sHA3 hydrogels (sHA3-+EDC/NHS) due to a lower amount of sHA3 which is already released during the washing procedure (Fig. 1 D). The volume increase of the scaffolds when incubated in PBS was highest for the EDC/NHS-crosslinked samples (EDC/NHS: 71± 31% and sHA3+EDC/NHS 71 ± 5%) and less than a half for the sHA3/PBS samples (30± 8%), while all three scaffolds had a comparable starting volume (sHA3/PBS: 17.8 ± 1.6 mm^3, EDC/NHS: 17.0 ± 0.2 mm^3 and sHA3+EDC/NHS: 17.5 ± 1.7 mm^3) (Fig. 1F). Mucograft® itself is not mechanically stable after incubation in PBS; hence values for VI and elastic modulus could not be determined. Interestingly, physically bound sHA3 alone (sHA3/PBS) already improves the stability of Mucograft® enabling the determination of VI and elastic modulus. However, the elastic modulus of sHA3/PBS hydrogels with 0.5 ± 0.3 kPa was around 5 times lower than that of EDC/NHS- crosslinked hydrogels (EDC/NHS: 2.4 ± 1.2 kPa and sHA3-+EDC/NHS: 2.7 ± 0.8 kPa), which displayed a higher elastic modulus due to additional crosslinks (Fig. 1G). The scaffold morphology after functionalization with sHA3 was examined via SEM (Fig. 2A–F). The collagen matrices comprise a compact layer (Fig. 2 A - C) and a spongy layer (Fig. 2 D - F). The scaffolds show their characteristic bilayered surface structure after lyophilization independent of the treatment with sHA3 and/or crosslinking reagents.

3.2. In vitro: platelet rich fibrin – biomaterial interaction and growth factor release

All the evaluated collagen matrix groups allowed the infiltration of
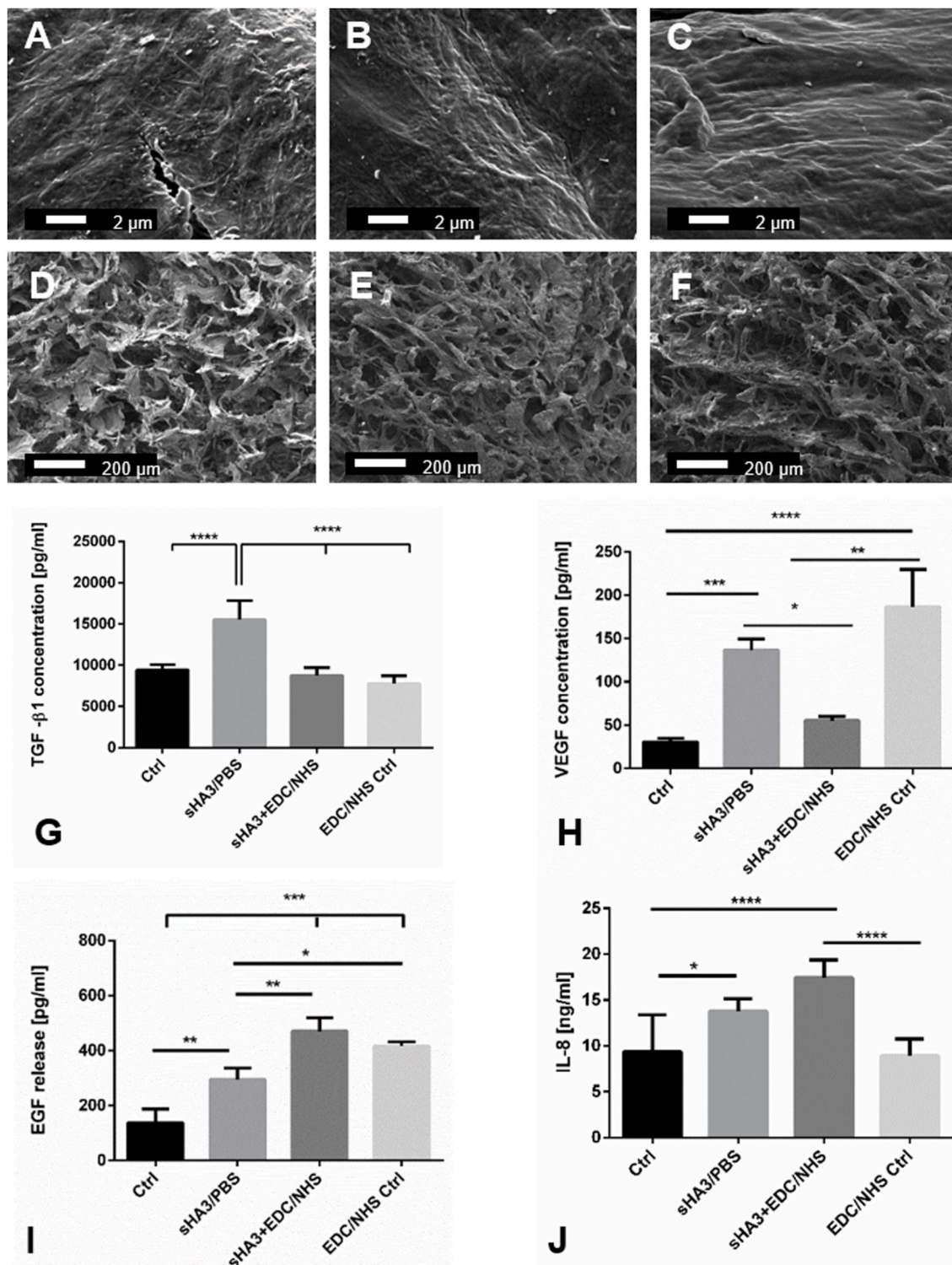
Fig. 2. Surface morphology of functionalized collagen-based scaffolds. SEM images of the low-porosity surface (A–C) and porous surface (D–F) of the collagen matrix are depicted after functionalization with sHA3 via noncovalent association (A, D), via covalent coupling (B, E) or after the crosslinking of collagen in the absence of sHA3 (C, F). G-J) Growth factors and cytokine release 3 days after cultivation with liquid platelet-rich fibrin. G) TGF-β1 release, H) VEGF release, I) EGF release and J) IL-8 release. Significant findings (*) with a p value < 0.05 and highly significant findings (**) with a p value < 0.01, (***) a p value < 0.001 or (****) a p value < 0.0001.

fibrin, platelets and leukocytes into the central region of the materials. Fibrin and cells were observed in both the spongy and compact layers (Supplementary Fig. 2). TGF-β1 release was the highest in the sHA3/PBS group. The difference was statistically significant compared to all the other groups (p < 0.0001), showing comparable concentrations of TGF-β1 without statistically significant differences (Fig. 2 G). VEGF release in the EDC/NHS Ctrl group was significantly higher than that in the Ctrl (p < 0.0001) and sHA3+EDC/NHS (p < 0.01) groups. The sHA3/PBS group released significantly higher VEGF than the Ctrl (p < 0.001) and sHA3+EDC/NHS groups (p < 0.05) (Fig. 2 H). A different pattern was

observed for the release of EGF. In this case, the highest concentration was released by the sHA3+EDC/NHS group, which was statistically significant compared to that released by the Ctrl ($p < 0.001$) and sHA3/PBS groups ($p < 0.01$). However, the sHA3/PBS group released significantly higher EGF concentrations than the Ctrl group ($p < 0.01$). The released EGF concentration of the EDC/NHS Ctrl group was significantly higher than that of the Ctrl group ($p < 0.001$) (Fig. 2 I). Interleukin 8 (IL-8) release was the highest in the sHA3+EDC/NHS group, which was statistically significant compared to that in the Ctrl ($p < 0.0001$) and EDC/NHS Ctrl ($p < 0.0001$) groups. The sHA3/PBS group released significantly higher concentrations of IL-8 than the Ctrl group ($p < 0.05$) (Fig. 2 J).

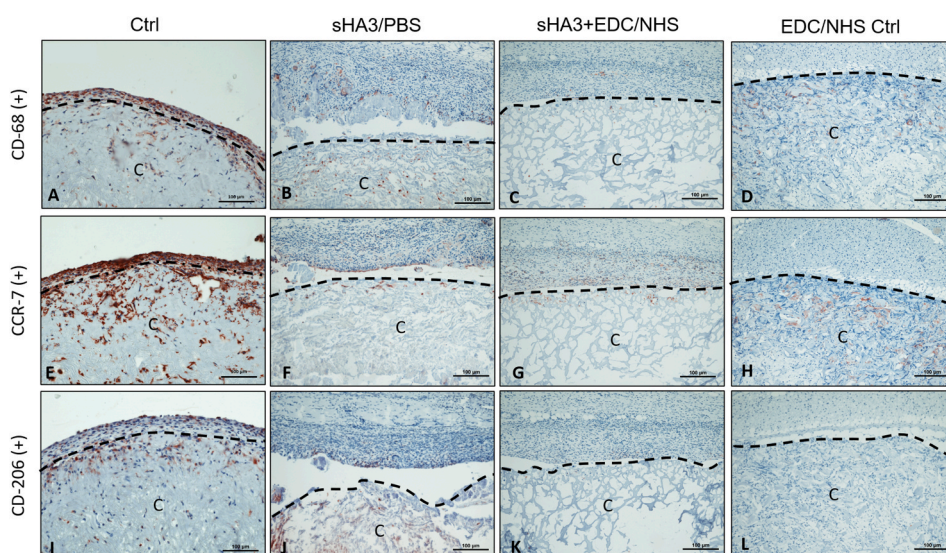### 3.3. In vivo cellular reaction to sHA3-functionalized collagen-based scaffolds

All animals recovered from the surgery without any complications. No adverse reactions, dehiscence or wound healing disorders were evident. Atypical feeding or sleeping behaviors were not observed in any group.

3.3.1. Morphological analysis of the cellular reaction to the different matrices

Mononuclear cells expressing CD-68 as a pan marker for macrophages, CCR-7 as a proinflammatory marker and CD-206 as an anti-inflammatory marker were assessed within the implantation region for the different evaluation time points over 30 days.

Three days after implantation, mononuclear cells accumulated in the surgery area in all groups. Macrophages (CD-68 (+)) of inflammatory type (CCR-7 (+)) accumulated on the peripheral surface of the implanted scaffolds and did not reach the central region of any group at this time point (Supplementary Fig. 3).

After 15 days, only mononuclear cells were observed in the groups Sham-OP, Ctrl and sHA3+EDC/NHS. The cells penetrated the peripheral superficial layers of the Ctrl group but did not reach the central region. Most of the observed cells were CD-68 (+) and CCR-7 (+). In the group of sHA3+EDC/NHS mononuclear cells were adherent on the scaffold surface but did not penetrate any area of the biomaterial. In the groups of sHA3/PBS and EDC/NHS Ctrl multinucleated giant cells (MNGCs) were detected in addition to the accumulated mononuclear cells. Both macrophages and MNGCs expressed CD-68, MMP-9 and CCR-7 rather than CD-206. The mononuclear cells invaded the peripheral parts of the scaffolds, whereas MNGCs were mainly located at the surface of the biomaterials in both groups (Fig. 3).
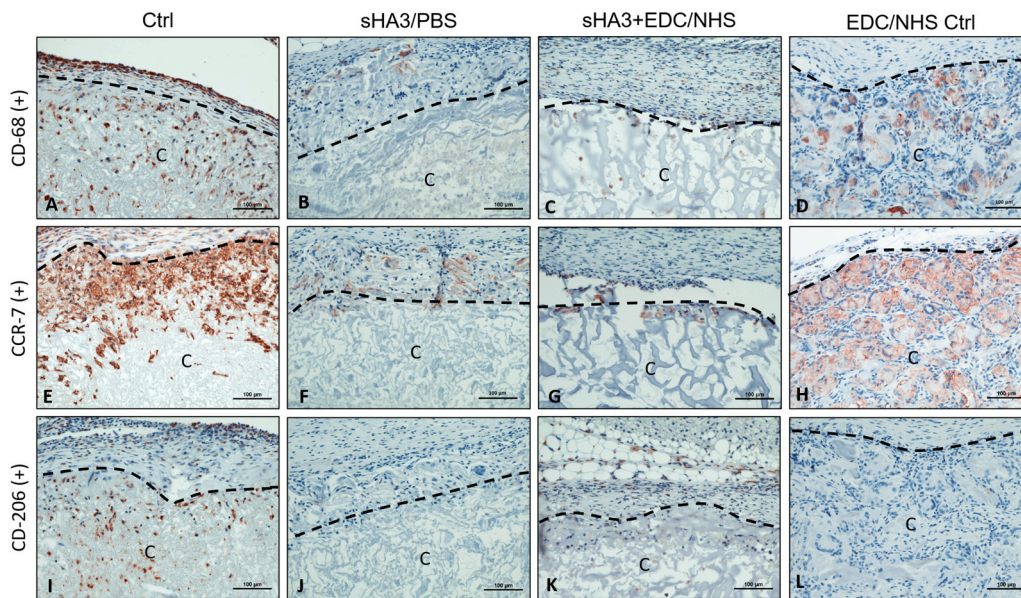
Thirty days after implantation, all materials were still detectable within the implantation area. The sham operation group was fully healed without any abnormal cellular reaction. No MNGCs were detected in the groups: Sham-OP, Ctrl and sHA3+EDC/NHS. Most of the mononuclear cells were CD-68 (+) and CCR-7 (+). They invaded the scaffold of the Ctrl group but did not destroy its initial structure. By contrast, sHA3+EDC/NHS showed a stable structure and was resistant to cellular invasion. Here, most cells observed were negative for CCR-7 and CD-68 and represented rather fibroblasts or endothelial cells. The sHA3/PBS group showed a higher number of MNGCs than that on day 15. MNGCs were mostly located at the biomaterial peripheral surface and were CCR-7 and MMP-9 positive. In the EDC/NHS Ctrl group, the biomaterial was fully penetrated by MNGCs. Almost all MNGCs expressed CCR-7 and MMP-9 but not CD-206. Additionally, the scaffolds lost their initial structure due to the penetration of these cells, which resulted in their breakdown and influx of connective tissue (Fig. 4A–L), (supplementary Fig. 6 A-D).

No material encapsulation was found for any scaffold at any time point. No TRAP-positive cells were found at any time point in any biomaterial.

3.3.2. Histomorphometric analyses of the cellular reaction over 30 days
The inflammatory pattern and the vascularization of the scaffolds were evaluated by histomorphometry for all time points to analyze inflammatory cell kinetics and biomaterial degradation.

3.3.2.1. Inflammatory activation of macrophages in response to the implanted biomaterials. Different inflammatory patterns were observed in the evaluated groups. Interestingly, the sHA3-EDC/NHS group induced the lowest number of inflammatory cells (CD-68 (+), CCR-(+), CD-206 (+)) at all the evaluated time points. Particularly after 3 days, the highest number of CD-68-positive cells was detected in the Ctrl group and the lowest number was detected in the sHA3+EDC/NHS group. The difference was statistically significant compared to the levels detected in the sHA3+EDC/NHS group (***$p < 0.0001$), EDC/NHS Ctrl group (***$p < 0.0001$) and the sham operation group (*$p < 0.05$). The sHA3/PBS samples showed a significantly higher number of CD-68-positive cells than the sHA3+EDC/NHS group (***$p < 0.0001$) and the EDC/NHS Ctrl group (***$p < 0.0001$). The number of CD-68-positive cells in the sham-OP group was significantly higher than that in the sHA3+EDC/NHS (***$p < 0.0001$) and EDC/NHS Ctrl (***$p < 0.0001$) groups. CCR-7-positive cells were highest in the Ctrl group. The difference was statistically significant compared to the sHA3/PBS (**$p <$

Fig. 3. *In vivo* cellular reaction to the collagen-based scaffolds 15 days after implantation. Immunohistological images showing different inflammatory patterns of the biomaterials and the appearance of multinucleated giant cells in sHA3/PBS and EDC/NHS Ctrl (A–D) CD-68+ cells, (E–H) CCR-7+ cells and (I–J) CD-206+ cells; all cells were stained red-brown. The black dashed line outlines the interface between the collagen matrix (C) and the peri-implantation area. All images were captured at x200 magnification. (For interpretation of the references to color in this figure legend, the reader is referred to the Web version of this article.)

Fig. 4. *In vivo* cellular reaction to the collagen-based scaffolds 30 days after implantation. Immunohistological pictures showing different inflammatory patterns of the biomaterials and an increased number of multinucleated giant cells in sHA3/PBS and EDC/NHS Ctrl (A–D) CD-68+ cells, (E–H) CCR-7+ cells and (I–J) CD-206+ cells; all cells were stained red-brown. The black dashed line outlines the interface between the collagen matrix (C) and the peri-implantation area All images were captured at x200 magnification. (For interpretation of the references to color in this figure legend, the reader is referred to the Web version of this article.)

0.01), sHA3+EDC/NHS (**p < 0.0001) and EDC/NHS Ctrl (**p < 0.01) groups. The sham-OP group induced a significantly higher number of CCR-7 positive cells than that induced by the sHA3/PBS (*p < 0.05), sHA3+EDC/NHS (****p < 0.0001) and EDC/NHS Ctrl (**p < 0.01) groups. The number of CD-206-positive cells was highest in the Ctrl group and lowest in the sHA3+EDC/NHS group. It was significantly lower than that in the Ctrl and Sham-Op groups (*p < 0.05 for both), (Fig. 5 A).

Fifteen days after implantation, the Ctrl group induced a high number of CD-68-positive cells, while the sHA3+EDC/NHS group induced the lowest number. The former was significantly higher than that induced by the sHA3+EDC/NHS (***p < 0.001), EDC/NHS Ctrl (***p < 0.001) and sham-OP (**p < 0.01) groups. The sHA3/PBS group showed a comparable number of CD-68 positive cells to that of the Ctrl group without a significant difference. However, the difference was statistically significant compared to that induced by the sHA3+EDC/NHS (****p < 0.0001), EDC/NHS Ctrl (****p < 0.0001) and sham-OP (***p < 0.001) groups. The sham-OP group induced a higher number of CD-68-positive cells than the sHA3+EDC/NHS and EDC/NHS Ctrl groups, but without statistically significant differences. The highest number of CCR-7-positive cells was detected in the EDC/NHS Ctrl group, and the lowest number was detected in the sHA3+EDC/NHS group. The number of CCR-7 positive cells in the EDC/NHS Ctrl group was significantly higher than that in the sHA3/PBS (****p < 0.0001), sHA3+EDC/NHS (****p < 0.0001), Ctrl (****p < 0.0001) and sham-OP (***p < 0.001) groups. The Ctrl group induced the highest number of CD-206-positive mononuclear cells, which was significantly higher than that induced by the sHA3/PBS (*p < 0.05), sHA3+EDC/NHS (*p < 0.05), and EDC/NHS Ctrl (*p < 0.05) groups but not significantly different compared to that of the sham-OP (Fig. 5 B) group. The HA3+EDC/NHS group induced the lowest number of CD-206 cells.

On day 30, a change in the inflammatory pattern was observed. The highest number of CD-68-positive cells was detected in the EDC/NHS Ctrl group. The number of CD-68-positive cells in the EDC/NHS Ctrl group was significantly higher than that in the Ctrl (***p < 0.001), sHA3/PBS (***p < 0.001), sHA3+EDC/NHS (****p < 0.0001) and sham-OP groups (****p < 0.0001). The number of CD-68-positive cells was significantly higher in the Ctrl group than that in the sHA3+EDC/NHS (**p < 0.01) group. The EDC/NHS Ctrl group showed the highest number of CCR-7-positive cells. It was significantly higher than that in the Ctrl (***p < 0.001), sHA3/PBS (***p < 0.001), sHA3+EDC/NHS (****p < 0.0001) and sham-OP groups (****p < 0.0001). Additionally,

the Ctrl group showed a relatively high number of CCR-7-positive cells that was comparable to the numbers found in the sHA3/PBS and sham-OP groups. The sHA3+EDC/NHS group showed the lowest number of CCR-7-positive cells, which was significantly lower than that of the Ctrl group (**p < 0.01). The numbers of CD-206-positive cells were comparable in all groups and showed no statistically significant differences (Fig. 5C–F).

3.3.2.2. Multinucleated giant cells formation. No multinucleated giant cells (MNGCs) were found in any group at the first observation time point (day 3). After 15 days, MNGCs were detected only in the sHA3/PBS and EDC/NHS Ctrl groups and were not observed in the Ctrl, sHA3+EDC/NHS and sham-OP groups. No TRAP-positive cells were detected at any time point; therefore, this marker was excluded from the histomorphometric analysis.

The number of CD-68-positive MNGCs was the highest in the EDC/NHS Ctrl group, which was highly significant compared to that of the Ctrl (****p < 0.0001), sHA3+EDC/NHS (****p < 0.0001), sham-OP (****p < 0.0001) and sHA3/PBS (*p < 0.05) groups. The number of CD-68-positive MNGCs in the sHA3/PBS group was significantly higher than that in the Ctrl (**p < 0.01), sHA3+EDC/NHS (**p < 0.01) and sham-OP groups (**p < 0.01). A high number of MNGCs expressed CCR-7 in the EDC/NHS Ctrl group, which was significantly higher than the number of cells observed in all the other groups (****p < 0.0001). Similarly the number of MMP-9-positive cells was the highest in the group of EDC/NHS Ctrl, which was significantly higher than the number of cells observed in all the other groups (****p < 0.0001). Only a few CCR-7-positive and MMP-9-positive MNGCs were found in the sHA3/PBS group. In contrast, a higher number of CD-206-positive cells was found in the sHA3/PBS group than in the EDC/NHS Ctrl group without a statistically significant difference (Fig. 6 I).

On day 30, the MNGC numbers increased in both the sHA3/PBS and EDC/NHS Ctrl groups. In contrast, the Ctrl, sHA3+EDC/NHS and sham-OP groups did not have any induced MNGCs at this time point. The number of CD-68-positive MNGCs in the former two groups was significantly higher than that in all the other groups (****p < 0.0001 and **p < 0.01). A similar pattern was found for CCR-7-positive and MMP-9-positive cells. A high number was found in the EDC/NHS Ctrl group, which was significantly higher than that observed in all the other evaluated groups (****p < 0.0001 for both). Additionally, a small number of MNGCs expressed CD-206 in the sHA3/PBS and EDC/NHS groups (Fig. 6 A-H and J).
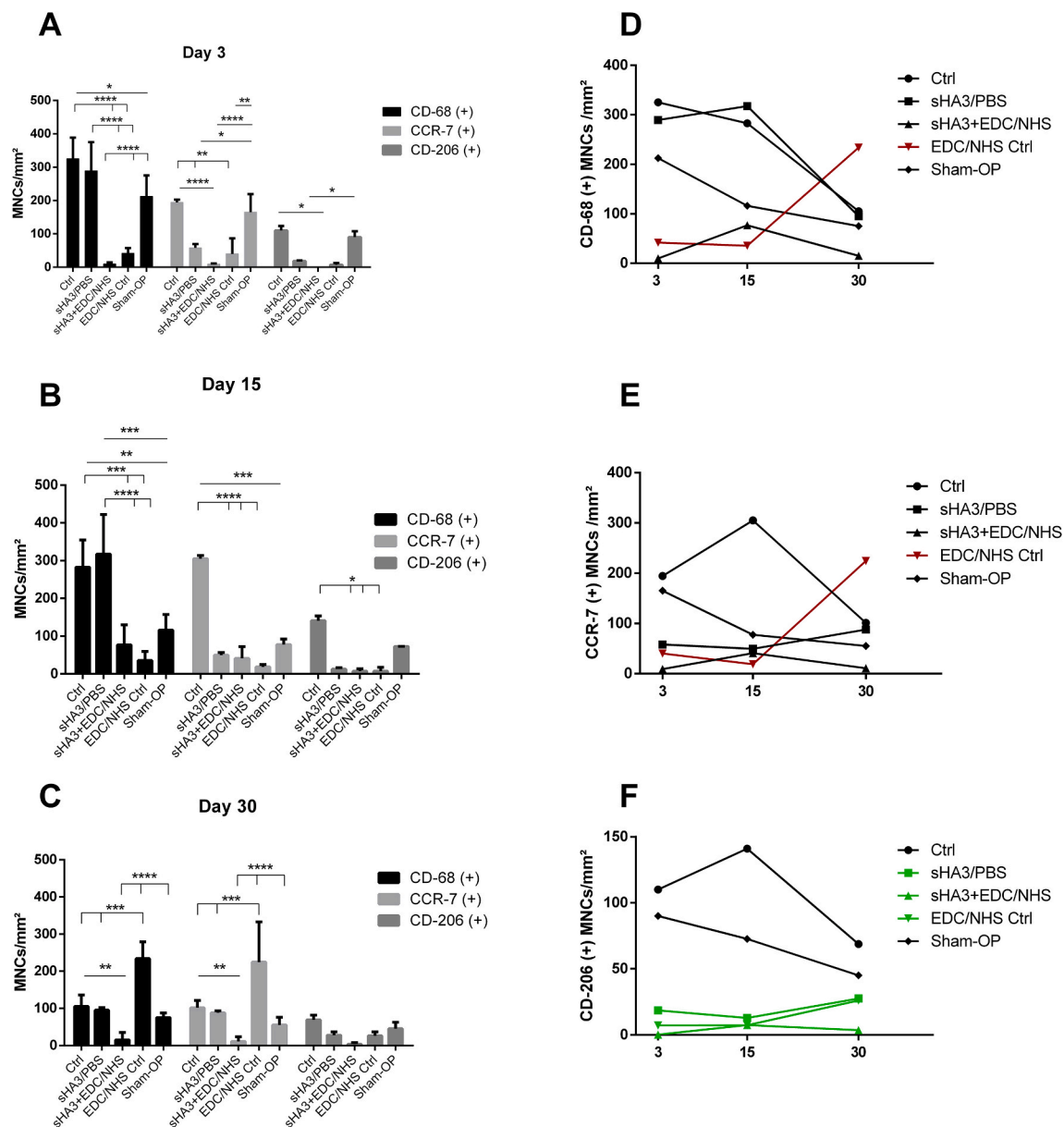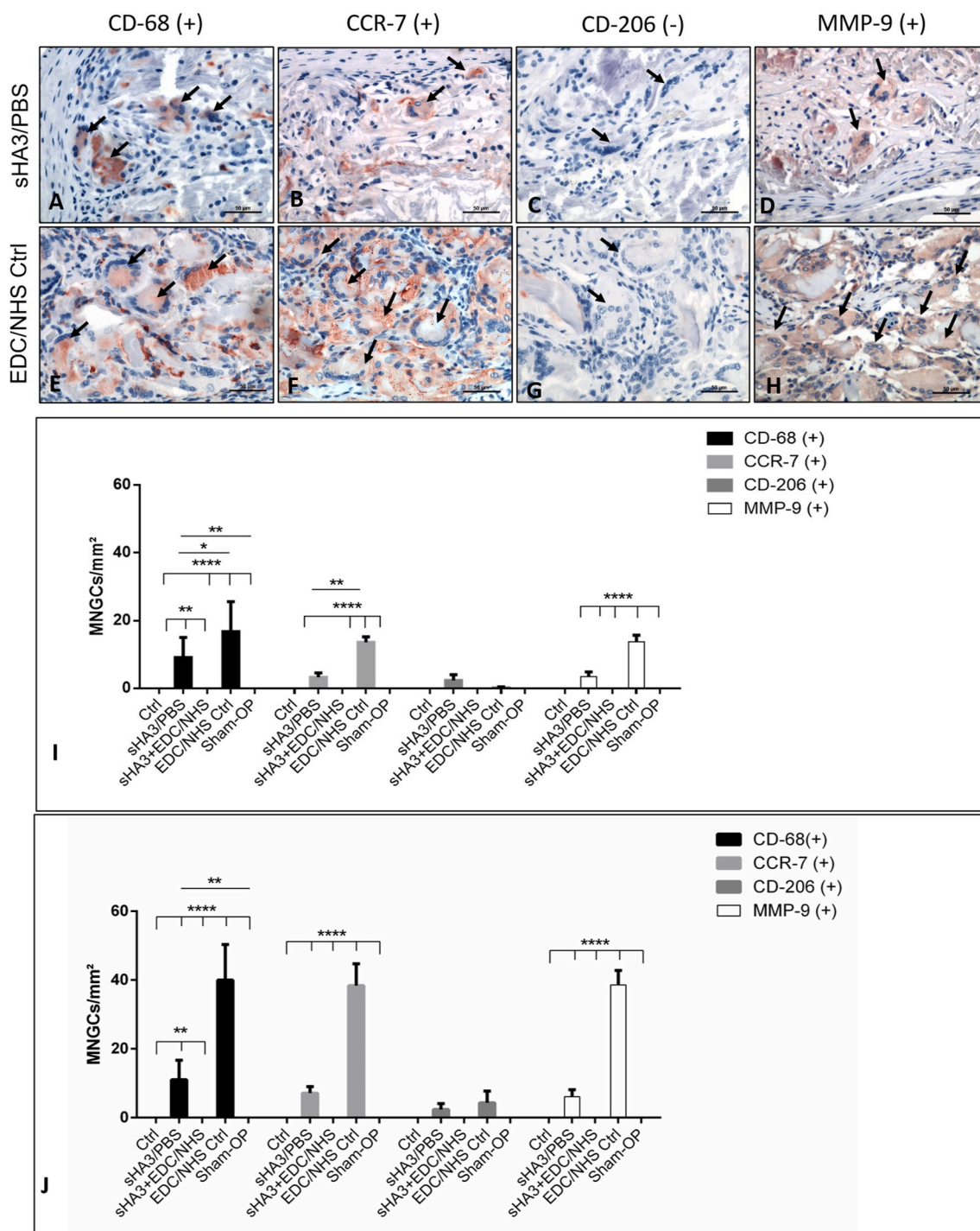
Fig. 5. *In vivo* **inflammatory pattern of mononuclear cells (MNCs) in response to different collagen-based biomaterials over 30 days.** Histomorphometric and statistical analyses after A) day 3, B) day 15, and C) day 30. D-F) The inflammatory kinetics of the differently activated mononuclear cells over 30 days. Significant findings (*) with a p value < 0.05 and highly significant findings (**) with a p value < 0.01, (***) a p value < 0.001 or (****) a p value < 0.0001.

3.3.2.3. Vascularization pattern. Three days after implantation, no vessel formation was found in any biomaterial. However, in the sham-OP group, a small number of vessels was detected. The number of vessels in the sham-OP group was not significantly higher than that detected in all the other groups. After fifteen days, vessel formation was detected in the EDC/NHS Ctrl group, this being mostly localized in the periphery. Their number was comparable to that observed in the sham-OP group. The EDC/NHS Ctrl group showed blood vessels within the biomaterial, especially in close relation to the MNGCs. Their density was significantly higher than the Ctrl (***p < 0.001), sHA3/PBS (***p < 0.001) and sHA3+EDC/NHS (***p < 0.001) groups. The vessel density of the sham-OP group was significantly higher than that of the Ctrl (*p < 0.05), sHA3/PBS (*p < 0.05) and sHA3+EDC/NHS (*p < 0.05) groups. After thirty days, the vessel density in the EDC/NHS Ctrl group was the highest. In this group, blood vessels were located at the biomaterial surface but not within the biomaterial body. The density was significantly higher than that in all the other evaluated groups (****p <

0.0001). It was significantly lower in the sHA3/PBS group than that in the sham-OP group (***p < 0.001) but was not significantly different from that in the Ctrl and sHA3+EDC/NHS groups. In contrast, the vessel density of the sham-OP group was significantly higher than that of the Ctrl (****p < 0.0001) and sHA3+EDC/NHS (****p < 0.0001) groups (Fig. 7A–E).

Additionally, there was a statistically significant increase in the vessel density over time, only in the EDC/NHS Ctrl group, from day 3–15 (●● p < 0.01) and from day 15–30 (●●●● p < 0.0001). Similarly, the vessel density increased significantly when comparing days 15–30 (●● p < 0.01), (Supplementary Fig. 5).

3.3.2.4. Degradation pattern. On day 3, the sHA3+EDC/NHS modifications and EDC/NHS Ctrl modifications showed biomaterial structures that were almost six times thicker. Biomaterial degradation was defined as the thickness reduction over time. In the Ctrl, sHA3/PBS and sHA3+EDC/NHS groups, no statistically significant differences were detected

Fig. 6. *In vivo inflammatory pattern of the induced multinucleated giant cells (MNGC) in response to different collagen-based scaffolds over 30 days.* Representative images of the observed MNGCs (black arrows), A-D) in the group of sHA3/PBS and E-H) in the group of EDC/NHS Ctrl on day 30 after *in vivo* implantation. Histomorphometric and statistical analyses after I) day 15 and J) day 30. Significant findings (*) with p value < 0.05 and highly significant findings (**) with a p value < 0.01, (***) a p value < 0.001 or (****) a p value < 0.0001.

in the thickness over the study period. However, the EDC/NHS Ctrl group revealed a thickness reduction from day 3 to day 15 without a significant difference. The difference was statistically significant from day 15 to day 30 (**p < 0.01). Additionally, the material thickness on day 30 was significantly lower than that on day 3 (***p < 0.001) (Fig. 8A–E).

4. Discussion

Different collagen-based materials are available for clinical applications, such as intraoral tissue regeneration [12,38] or full-thickness skin regeneration [39]. However, many limitations are faced concerning their biomaterial-induced high inflammatory cellular reactions, biomaterial degradation patterns and degradation time periods [40].

This study was performed to analyze the regenerative capacity of a collagen-based scaffold after biomaterial functionalization using sHA3.
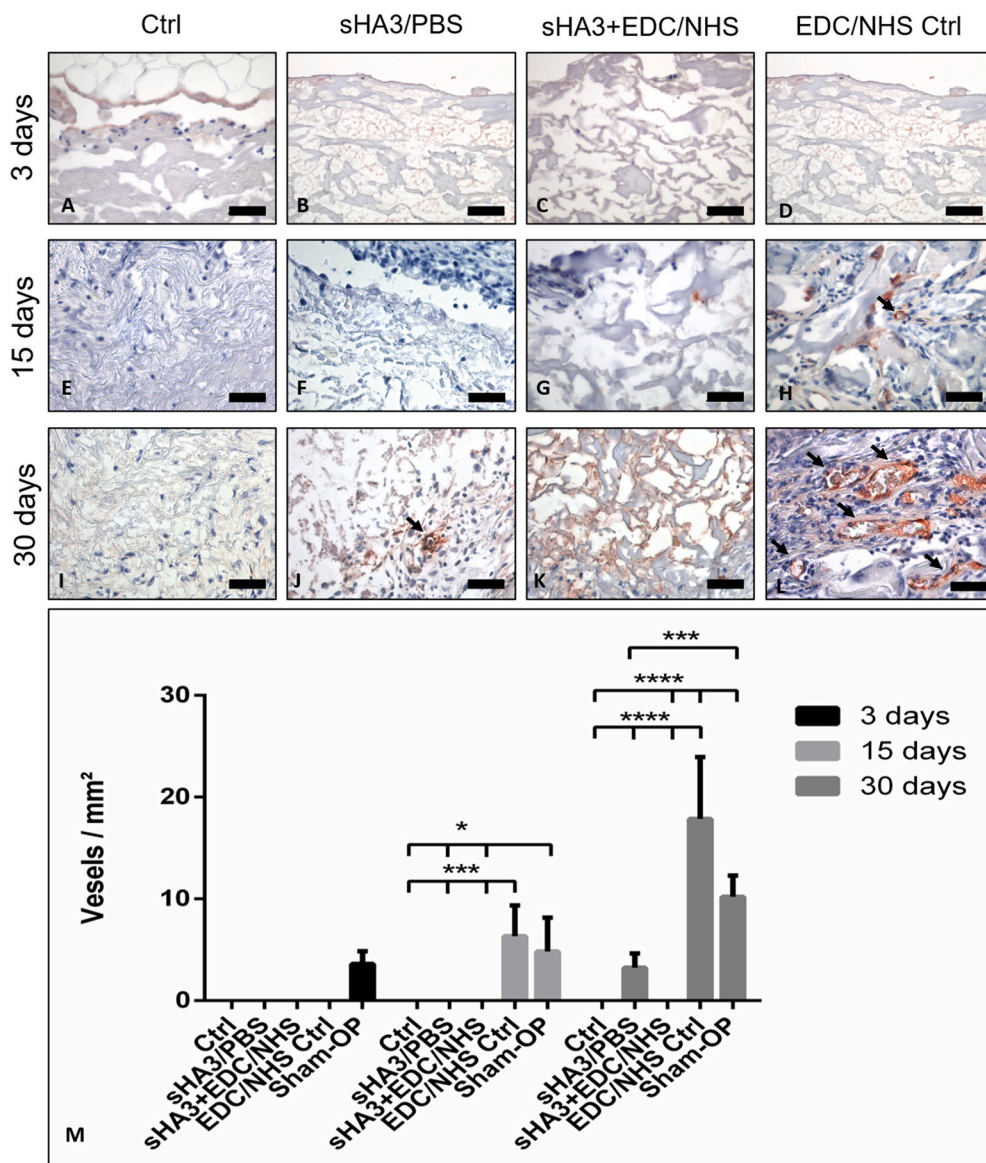
Fig. 7. Vascularization over 30 days after the implantation of different collagen-based scaffolds *in vivo*. Immunohistochemical staining highlights Von Willebrand Factor-positive structures in a red-brown color. Vascularization pattern is presented at different time points A-D) day 3 E-H) day 15 and I-L) day 30. Arrows point to vessel structures within the biomaterial body. All images were captured at x400 magnification. M) Histomorphometric and statistical analysis of the vessel density of the collagen-based materials over 30 days. Significant findings (*) with a p value < 0.05 and highly significant findings (**) with a p value < 0.01, (***) a p value < 0.001 or (****) a p value < 0.0001. (For interpretation of the references to color in this figure legend, the reader is referred to the Web version of this article.)
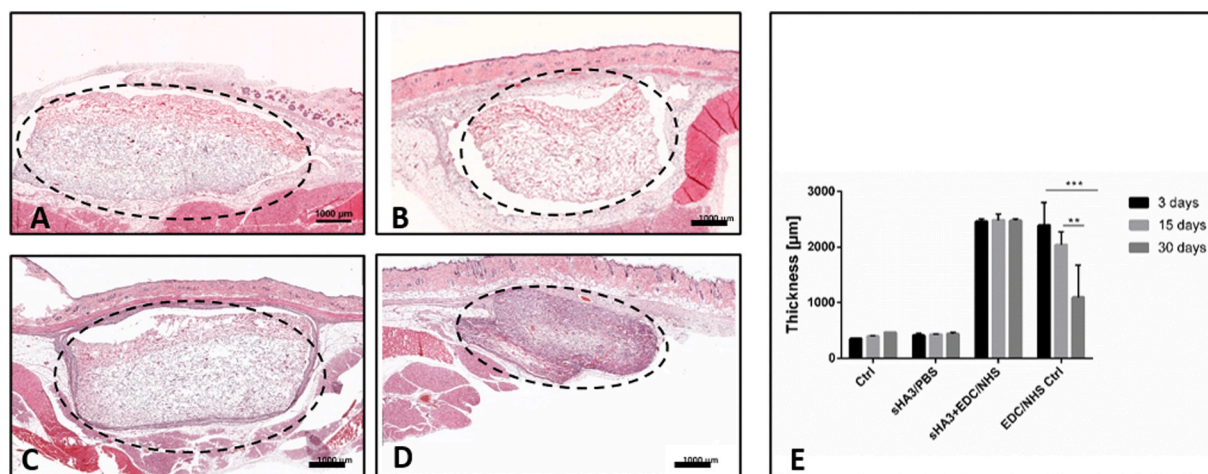
Fig. 8. *In vivo* degradation patterns of different collagen-based scaffolds over 30 days *in vivo*.
The material thickness on day 3 of A) sHA3+EDC/NHS and B) EDC/NHS Ctrl and the thickness on day 30 of C) sHA3+EDC/NHS and D) EDC/NHS Ctrl. Images were captured at x40 magnification for total hematoxylin and eosin staining. E) Histomorphometric and statistical analysis of the thickness reduction of the collagen-based materials over 30 days. Findings were highly significant (**) with p values < 0.01 and (***) p values < 0.001.

Three different types of modification of collagen-based matrices were characterized and evaluated *in vitro* and *in vivo* to elucidate the impact of sHA3 on the inflammatory response, vascularization, and degradation patterns of the scaffolds.

Hydrogels containing sHA3 were shown to function as growth factor reservoirs and to provide a suitable microenvironment for proliferating cells [25]. Previous *in vitro* studies recently demonstrated that the addition of hyaluronan to the extracellular matrix leads to a decrease in monocyte differentiation into macrophages [41]. Moreover, sHA3 was shown to reduce the proinflammatory release of tumor necrosis factor-alpha and thereby inhibit the proinflammatory activation of macrophages *in vitro* [28].

Using a mixture of EDC and NHS, Wissink et al. achieved a collagen crosslinking degree of approximately 52% [5], which is lower than that observed in our study in which we used EDC/NHS concentrations that were more than two times higher. However, when also using an EDC/NHS ratio of 0.5 and the GAG heparin, the authors likewise immobilized approximately 25 µg GAG per mg, suggesting that the amount of covalently bound GAG is related to the efficiently activated carboxylic groups and not to the GAG type present. Collagen matrices with covalently tethered sHA3 showed only a marginal sHA3 release over time. In contrast, a continuous release of sHA3 was observed from samples treated with sHA3/PBS in the absence of carbodiimides (even though their sHA3 content was comparable (2–2.5 wt%) after 1 h of incubation in PBS). This finding highlights the stabilizing effects of crosslinking documented by the percent of remaining sHA3 after up to 28 days. In addition, our findings show that crosslinked sHA3 was still able to interact with mediator proteins.

Biomaterials are mainly implanted in a surgically prepared wound, thus the first contact between the biomaterial and the host tissue occurs through blood. In this study, a blood concentrate (liquid PRF) [35] was used to simulate this phase and to evaluate the interaction of the differently modified collagen matrices with blood cells (platelets, leukocytes and lymphocytes). After 3 days, TGF-β1 was highest in the supernatants of sHA3/PBS, whereas the highest concentrations of VEGF were detected in both the sHA3/PBS and EDC/NHS Ctrl groups. The release of EGF and IL-8 was highest in the sHA3+EDC/NHS group. This biomaterial-dependent growth factor and cytokine release pattern may be explained in two ways. First, cellular activation occurs in response to the modified biomaterial surface to release different growth factors. Second, sHA3 affects the biomaterial surface and the cells included in liquid PRF. Sulfated HA was shown to strongly bind to VEGF-A and TGF-β1 [42,43]. Interestingly, VEGF and TGF-β1, the sHA3+EDC/NHS group that contained the highest amounts of the functionalized sHA3 scaffolds showed lower growth factor release than the other groups. Most likely, the concentration detected here may not reflect the total amount of these mediator proteins because significant protein amounts should remain bound to sHA3 within the matrix. In contrast, the highest concentration of released EGF was found for the sHA3+EDC/NHS group. Since EGF does not interact with sHA3, as demonstrated by SPR, any EGF retardation by sHA3 within the biomaterial can be excluded, which suggests a cell stimulating effect of covalently linked sHA3 during the production of EGF. In the case of IL-8, the release by lymphocytes and macrophages in the liquid PRF was enhanced by the interaction with sHA3. A previous study has shown that the combination of a collagen matrix with a different blood concentrate system PRP leads to increased angiogenesis and vascularization. Moreover, this combination led to a lower release of the pro-inflammatory marker MIP-1α and an increased release of the anti-inflammatory marker IL-1 [44]. Therefore, the sHA3-functionalized scaffolds loaded with liquid PRF have a high potential to enhance wound healing.

After the first blood contact with the biomaterial in the recipient area, the host cells react to the applied biomaterial, leading to a specific biomaterial-induced cellular reaction that may predefine and influence its regenerative capacity [45,46]. In this study, the focus was placed on the type of induced cells by the different scaffolds and the expression pattern of pro- and anti-inflammatory molecules. Interestingly, our findings demonstrated a different inflammatory dynamic in the groups Ctrl, sHA3/PBS and sham-OP, showing decreasing numbers of inflammatory cells from day 3–30 in the sham- op group compared to the increasing number of inflammatory cells in the groups sHA3/PBS and EDC/NHS Ctrl. This pattern may be related to chronic inflammation by the recruitment of a high number of proinflammatory cells in response to the implanted crosslinked scaffold [47]. Interestingly, in the sHA3-+EDC/NHS group, the number of CD-68- and CCR-7-positive proinflammatory cells was constant over time. This pattern suggests that the implanted material resulted in a reduction of the proinflammatory cell number by crosslinked sHA. Notably, the sHA3/PBS group, which contained lower amounts of sHA3, did not show an inhibitory effect on proinflammatory mononuclear cells. These results highlight the importance of the technique used for biomaterial functionalization with sHA3. Physically bound sHA3 in the sHA3/PBS group showed a high initial release of sHA3. In contrast, the covalent binding of sHA3 to collagen in the sHA3+EDC/NHS led to a low release of sHA3 over 28 days and higher amounts of scaffold-bound sHA3 as well. In this context, sHA3 could utilize its anti-inflammatory capability *in vivo* in the sHA3-+EDC/NHS group. Remarkably, sHA3 did not show a supportive effect on CD-206 anti-inflammatory macrophages in either group. However, in the present study, only one marker for each macrophage phenotype was evaluated. Within this limitation, it is likely that other pro- or anti-inflammatory signaling molecules, e.g., Cox-2 and iNOS or CD-163 or CD-86, may have shown an altered expression pattern. This remains to be determined.

The sHA3/PBS and EDC/NHS Ctrl groups showed the formation of multinucleated giant cells (MNGCs) beginning with day 15 and continuing thereafter with increasing numbers. Previous studies reported that the induction of MNGCs takes place during a chronic inflammatory reaction and is due to the fusion of macrophages [47–49]. A series of studies showed that the induction of these cells was evident regardless of the biomaterial origin, i.e., natural or synthetic [50], but depends primarily on biomaterial related physicochemical properties, such as porosity [11], thickness [51], chemical preparation techniques [52,53], and surface characteristics, including hydrophilic capacity [54]. The electrostatic loading of sHA3 did not lead to a sustained release over 30 days, as documented by the sHA3 release evaluation over 28 days (Fig. 1). This means the release of sHA3 in this group subsided after 15 days *in vivo*. The resulted scaffold however, did not show the same inflammatory pattern as the non-modified Ctrl. By contrast sHA3/PBS induced the formation of MNGCs starting on day 15. This interesting finding may be explained by changes in the surface structure, that might have taken place by the treatment with sHA3 in terms of changes in the collagen fibers. In previous studies it was shown that the presence of sHA modified the fibrillar structure of collagen when incubated during *in vitro* fibrillogenesis [55]. Thus, it might be concluded that after the release of sHA3, the remaining modified scaffold (sHA3/PBS) is not the same as the native non-modified Mucograft (Ctrl). Surface structure is one of the most important factors modulating the formation of MNGCs, as documented by previous studies [56,57].

These findings support the hypothesis that sHA3 may suppress the induction of MNGCs *in vivo*. Similarly, this aspect is clearly observable in the other evaluated groups, especially crosslinking via EDC/NHS induced a high number of MNGCs, while the same material, which was modified using sHA3+EDC/NHS, did not induce any MNGCs. This aspect may be in addition to the anti-inflammatory effect of sHA3 caused by the zeta potential of the biomaterial surface that was shown to be changed due to negatively charged sHA3 [58]. As a result, the biomaterial surface has the capacity to bind positively charged proteins, which is a trend-setting effect for the following inflammatory pattern. The effect of the biomaterial surface was demonstrated to have an impact on the foreign body reaction [54]. The adsorbed proteins on the biomaterial surface predefine the interface between the implanted biomaterial and the recipient tissue, which provides the initial possibility for the immune

cells to communicate with the introduced surface [59]. Additionally, it was previously shown that an enhanced hydrophilic capacity of biomaterials leads to a reduction in the macrophage number and thereby inhibition of their fusion to form MNGCs [60,61]. The hydrophilic nature of the sHA3 used here may have led to a similar effect and thereby inhibited the formation of MNGCs in the sHA3+EDC/NHS group compared to that observed in the EDC/NHS Ctrl group. The covalent binding of sHA3 to collagen strongly preserved this property compared to the noncovalent association of sHA3 in the sHA3/PBS group. However, the latter induced a significantly lower number of MNGCs than the EDC/NHS Ctrl group. These findings substantiate the hypothesis that covalently bound sHA3 reduced the formation of MNGCs. Additionally, these observations support the hypothesis that chemical crosslinking may lead to a stable structure, but this method mostly results in a chronic inflammatory reaction induction of foreign body giant cells, while the non-crosslinked Ctrl did not induce any MNGCs. Similarly, some studies have shown that chemical crosslinking results in a stable physical structure, but a high inflammatory reaction and even faster degradation *in vivo* [62,63]. Most of the analyzed MNGCs expressed the proinflammatory marker CCR-7, whereas only a few MNGCs expressed CD-206 as an anti-inflammatory marker. Similar findings were previously presented in an analysis of human biopsies including two individual bone substitute materials that induced MNGCs. In this cited study, a high number of the induced MNGCs expressed proinflammatory markers such as CCR-7 and Cox-2 [64]. Additionally, a high number of MNGCs expressed MMP-9. The expression of MMP-9 was previously evident in disease related MNGCs (e.g. tuberculosis) [65]. Moreover, it was shown to be involved in the inflammatory process of MNGCs formation [66]. As a matrix metalloproteinase, a high expression of MMP-9 can result into extensive extracellular matrix degradation, especially collagen in different regions of the body [67]. Thereby, the high expression of MMP-9 in the groups of sHA3/PBS and EDC/NHS Ctrl may explain the high *in vivo* degradation of these groups and the enhanced *in vivo* stability of sHA3+EDC/NHS, in which MNGCs were not evident over the study period.

Crosslinking is thought to enhance the mechanical stability and also enhance the degradation resistance of collagen-based biomaterials [17]. In line with this, our results showed a very stable structure in the EDC/NHS Ctrl group with significantly reduced release levels, higher amounts of preserved collagen after 28 days and higher elastic modulus compared to the PBS/sHA3 group. However, these findings were not mirrored *in vivo*. This is because of the limitation of the characterization model used here. As scaffold incubation was performed to compare the results with previous studies on sHA3-containing biomaterials in the absence of proteases, this system cannot mimic the natural *in vivo* microenvironment. Moreover, the collagen degradation observed in the EDC/NHS Ctrl group may have occurred due to cellular processes represented by MNGCs in addition to the enzymatic degradation of the host tissue.

Based on the obtained results, the material modification presented here for sHA3+EDC/NHS showed favorable characteristics in terms of material stability, inflammatory reaction, and growth factor release, that represent the most critical factors for wound healing and scar formation. Therefore, the presented material may fulfill the clinical requirements needed for full-thickness skin regeneration or chondral regeneration by supporting the regeneration process and reducing scar formation. However, these promising results need further verification in different animal models.

5. Conclusion

The present study evaluated three different types of modification of a clinically used collagen-based matrix. The evaluated groups included different sHA3 associations (sHA3/PBS and sHA3+EDC/NHS) and an EDC/NHS Ctrl group for which the materials were characterized and growth factor release *in vitro* and inflammatory and degradation patterns

in vivo were analyzed. The results demonstrate the promising potential of covalently bound sHA3 (sHA3+EDC/NHS) to provide a physically stable collagen-based structure, controlled growth factor release *in vitro* and reduced induced inflammatory pattern without the formation of MNGCs *in vivo*. These findings suggest that the technique presented here has high potential for applications in full-thickness skin regeneration. However, further verification in different animal models is needed to prove whether these features may lead to optimized wound healing by providing a stable scaffold, enhancing epithelialization and reducing scar formation.

Declaration of competing interest

The authors declare that they have no conflict of interest.

Acknowledgments

Appendix A. Supplementary data

Supplementary data to this article can be found online at https://doi.org/10.1016/j.bioactmat.2021.06.008.

References

[1] M. Minabe, A critical review of the biologic rationale for guided tissue regeneration, J. Periodontol. 62 (1991) 171–179, https://doi.org/10.1902/jop.1991.62.3.171.

[2] I. Elgali, A. Turri, W. Xia, B. Norlindh, A. Johansson, C. Dahlin, P. Thomsen, O. Omar, Guided bone regeneration using resorbable membrane and different bone substitutes: early histological and molecular events, Acta Biomater. 29 (2016) 409–423, https://doi.org/10.1016/j.actbio.2015.10.005.

[3] S. Ghanaati, A. Kovcs, M. Barbeck, J. Lorenz, A. Teiler, N. Sadeghi, C.J. Kirkpatrick, R. Sader, Bilayered, non-cross-linked collagen matrix for regeneration of facial defects after skin cancer removal: a new perspective for biomaterial-based tissue reconstruction, J. Cell Commun. Signal. 10 (2016) 3, https://doi.org/10.1007/s12079-015-0313-7.

[4] P. Chia-Lai, A. Orlowska, S. Al-Maawi, A. Dias, Y. Zhang, X. Wang, N. Zender, R. Sader, C.J. Kirkpatrick, S. Ghanaati, Sugar-based collagen membrane cross-linking increases barrier capacity of membranes, Clin. Oral Invest. (2017), https://doi.org/10.1007/s00784-017-2281-1.

[5] J.S. Boateng, K.H. Matthews, H.N.E. Stevens, G.M. Eccleston, Wound healing dressings and drug delivery systems: a review, J. Pharm. Sci. 97 (2008) 2892–2923, https://doi.org/10.1002/jps.21210.

[6] M. Barbeck, J. Lorenz, A. Kubesch, N. Böhm, P. Booms, J. Choukroun, R. Sader, C. J. Kirkpatrick, S. Ghanaati, Porcine dermis-derived collagen membranes induce implantation bed vascularization via multinucleated giant cells: a physiological reaction? J. Oral Implantol. 41 (2015) e238–e251, https://doi.org/10.1563/aaid-joi-D-14-00274.

[7] S. Al-Maawi, J. Rutkowski, R. Sader, C.J. Kirkpatrick, S. Ghanaati, The biomaterial-induced cellular reaction allows a novel classification system regardless of the biomaterials origin, J. Implantol. 46 (3) (2020) 190–207, https://doi.org/10.1563/aaid-joi-D-19-00201.

[8] S. Al-Maawi, A. Orlowska, R. Sader, C. James Kirkpatrick, S. Ghanaati, In vivo cellular reactions to different biomaterials—physiological and pathological aspects and their consequences, Semin. Immunol. 29 (2017) 49–61, https://doi.org/10.1016/j.smim.2017.06.001.

[9] S. Ghanaati, Non-cross-linked porcine-based collagen I-III membranes do not require high vascularization rates for their integration within the implantation bed: a paradigm shift, Acta Biomater. 8 (2012) 3061–3072, https://doi.org/10.1016/j.actbio.2012.04.041.

[10] J. Brinkmann, T. Hefti, F. Schlottig, N.D. Spencer, H. Hall, Response of osteoclasts to titanium surfaces with increasing surface roughness: an in vitro study, Biointerphases 7 (2012) 34, https://doi.org/10.1007/S13758-012-0034-X.

[11] S. Ghanaati, M. Barbeck, C. Orth, I. Willershausen, B.W. Thimm, C. Hoffmann, A. Rasic, R.A. Sader, R.E. Unger, F. Peters, C.J. Kirkpatrick, Influence of ??-tricalcium phosphate granule size and morphology on tissue reaction in vivo, Acta Biomater. 6 (2010) 4476–4487, https://doi.org/10.1016/j.actbio.2010.07.006.

[12] S. Ghanaati, M. Schlee, M.J. Webber, I. Willershausen, M. Barbeck, E. Balic, C. Görlach, S.I. Stupp, R. a Sader, C.J. Kirkpatrick, Evaluation of the tissue reaction

to a new bilayered collagen matrix in vivo and its translation to the clinic, Biomed. Mater. 6 (2011), 015010, https://doi.org/10.1088/1748-6041/6/1/015010.

[13] G. Lay, Y. Poquet, P. Salek-Peyron, M.-P. Puissegur, C. Botanch, H. Bon, F. Levillain, J.-L. Duteyrat, J.-F. Emile, F. Altare, Langhans giant cells from *M. tuberculosis* -induced human granulomas cannot mediate mycobacterial uptake, J. Pathol. 211 (2007) 76–85, https://doi.org/10.1002/path.2092.

[14] R.J. Miron, D.D. Bosshardt, Multinucleated giant cells: good guys or bad guys? Tissue Eng. B Rev. 24 (2018) 53–65, https://doi.org/10.1089/ten.TEB.2017.0242.

[15] P. Bunyaratavej, H.L. Wang, Collagen membranes: a review, J. Periodontol. 72 (2001) 215–229, https://doi.org/10.1902/jop.2001.72.2.215.

[16] A.K. McNally, J.M. Anderson, Macrophage fusion and multinucleated giant cells of inflammation, Adv. Exp. Med. Biol. 713 (2011) 97–111, https://doi.org/10.1007/978-94-007-0763-4_7.

[17] L.M. Delgado, Y. Bayon, A. Pandit, D.I. Zeugolis, To cross-link or not to cross-link? Cross-linking associated foreign body response of collagen-based devices, Tissue Eng. B Rev. 21 (2015) 298–313, https://doi.org/10.1089/ten.TEB.2014.0290.

[18] C. Dollinger, S. Ciftci, H. Knopf-Marques, R. Guner, A.M. Ghaemmaghami, C. Debry, J. Barthes, N.E. Vrana, Incorporation of resident macrophages in engineered tissues: multiple cell type response to microenvironment controlled macrophage-laden gelatine hydrogels, J. Tissue Eng. Regen. Med. 12 (2018) 330–340, https://doi.org/10.1002/term.2458.

[19] S. Prokop, F.L. Heppner, H.H. Goebel, W. Stenzel, M2 polarized macrophages and giant cells contribute to myofibrosis in neuromuscular sarcoidosis, Am. J. Pathol. 178 (2011) 1279–1286, https://doi.org/10.1016/j.ajpath.2010.11.065.

[20] B.N. Brown, J.E. Valentin, A.M. Stewart-Akers, G.P. McCabe, S.F. Badylak, Macrophage phenotype and remodeling outcomes in response to biologic scaffolds with and without a cellular component, Biomaterials 30 (2009) 1482–1491, https://doi.org/10.1016/j.biomaterials.2008.11.040.

[21] C. Frantz, K.M. Stewart, V.M. Weaver, The extracellular matrix at a glance, J. Cell Sci. 123 (2010) 4195–4200, https://doi.org/10.1242/jcs.023820.

[22] S.M. Sweeney, C.A. Guy, G.B. Fields, J.D. San Antonio, Defining the domains of type I collagen involved in heparin- binding and endothelial tube formation, Proc. Natl. Acad. Sci. U.S.A. 95 (1998) 7275–7280, https://doi.org/10.1073/pnas.95.13.7275.

[23] A. Miron, S. Rother, L. Huebner, U. Hempel, I. Käppler, S. Moeller, M. Schnabelrauch, D. Scharnweber, V. Hintze, K. Iris, S. Moeller, M. Schnabelrauch, D. Scharnweber, V. Hintze, Sulfated hyaluronan influences the formation of artificial extracellular matrices and the adhesion of osteogenic cells, Macromol. Biosci. 14 (2014) 1783–1794, https://doi.org/10.1002/mabi.201400292.

[24] M.J.B. Wissink, R. Beernink, J.S. Pieper, A.A. Poot, G.H.M. Engbers, T. Beugeling, W.G. van Aken, J. Feijen, Immobilization of heparin to EDC/NHS-crosslinked collagen. Characterization and in vitro evaluation, Biomaterials 22 (2001) 151–163.

[25] S. Rother, V.D. Galiazzo, D. Kilian, K.M. Fiebig, J. Becher, S. Moeller, U. Hempel, M. Schnabelrauch, J. Waltenberger, D. Scharnweber, V. Hintze, Hyaluronan/collagen hydrogels with sulfated hyaluronan for improved repair of vascularized tissue tune the binding of proteins and promote endothelial cell growth, Macromol. Biosci. (2017) 1–13, https://doi.org/10.1002/mabi.201700154, accepted.

[26] A. van der Smissen, V. Hintze, D. Scharnweber, S. Moeller, M. Schnabelrauch, A. Majok, J.C. Simon, U. Anderegg, Growth promoting substrates for human dermal fibroblasts provided by artificial extracellular matrices composed of collagen I and sulfated glycosaminoglycans, Biomaterials 32 (2011) 8938–8946, https://doi.org/10.1016/j.biomaterials.2011.08.025.

[27] D. Scharnweber, L. Hübner, S. Rother, U. Hempel, U. Anderegg, S.A. Samsonov, M. T. Pisabarro, L. Hofbauer, M. Schnabelrauch, S. Franz, J. Simon, V. Hintze, Glycosaminoglycan derivatives: promising candidates for the design of functional biomaterials, J. Mater. Sci. Mater. Med. 26 (2015) 232, https://doi.org/10.1007/s10856-015-5563-7.

[28] J. Kajahn, S. Franz, E. Rueckert, I. Forstreuter, V. Hintze, S. Moeller, J.C. Simon, Artificial extracellular matrices composed of collagen I and high sulfated hyaluronan modulate monocyte to macrophage differentiation under conditions of sterile inflammation, Biomatter 2 (2012) 226–236, https://doi.org/10.4161/biom.22855.

[29] S. Franz, F. Allenstein, J. Kajahn, I. Forstreuter, V. Hintze, S. Möller, J.C. Simon, Artificial extracellular matrices composed of collagen i and high-sulfated hyaluronan promote phenotypic and functional modulation of human pro-inflammatory M1 macrophages, Acta Biomater. 9 (2013) 5621–5629, https://doi.org/10.1016/j.actbio.2012.11.016.

[30] V. Hintze, S. Moeller, M. Schnabelrauch, S. Bierbaum, M. Viola, H. Worch, D. Scharnweber, Modifications of hyaluronan influence the interaction with human bone morphogenetic protein-4 (hBMP-4), Biomacromolecules 10 (2009) 3290–3297, https://doi.org/10.1021/bm9008827.

[31] R.W. Farndale, D.J. Buttle, A.J. Barrett, Improved quantitation and discrimination of sulphated glycosaminoglycans by use of dimethylmethylene blue, Biochim. Biophys. Acta 883 (1986) 173–177, https://doi.org/10.1016/0304-4165(86)90306-5.

[32] O.H. Lowry, N.J. Rosebrough, A.L. Farr, R.J. Randall, Protein measurement with the Folin phenol reagent, J. Biol. Chem. 193 (1951) 265–275, https://doi.org/10.1007/s10982-008-9035-9.

[33] C.-L. Wang, T. Miyata, B. Weksler, A.L. Rubin, K.H. Stenzel, Collagen-induced platelet aggregation and release. I Effects of side-chain modifications and role of arginyl residues, Biochim. Biophys. Acta 544 (1978) 555–567.

[34] W.A. Bubnis, C.M. Ofner, The determination of epsilon-amino groups in soluble and poorly soluble proteinaceous materials by a spectrophotometric method using trinitrobenzenesulfonic acid, Anal. Biochem. 207 (1992) 129–133, https://doi.org/10.1016/0003-2697(92)90513-7.

[35] J. Choukroun, S. Ghanaati, Reduction of relative centrifugation force within injectable platelet-rich-fibrin (PRF) concentrates advances patients' own inflammatory cells, platelets and growth factors: the first introduction to the low speed centrifugation concept, Eur. J. Trauma Emerg. Surg. 44 (2018) 87–95, https://doi.org/10.1007/s00068-017-0767-9.

[36] E. Dohle, K. El Bagdadi, R. Sader, J. Choukroun, C. James Kirkpatrick, S. Ghanaati, PRF-based matrices to improve angiogenesis in an *in vitro* co-culture model for bone tissue engineering, J. Tissue Eng. Regen. Med. (2017), https://doi.org/10.1002/term.2475.

[37] C. Kilkenny, W.J. Browne, I.C. Cuthill, M. Emerson, D.G. Altman, Improving bioscience research reporting: the ARRIVE guidelines for reporting animal research, PLoS Biol. 8 (2010), e1000412, https://doi.org/10.1371/journal.pbio.1000412.

[38] J. Lorenz, M. Blume, M. Barbeck, A. Teiler, C.J. Kirkpatrick, R.A. Sader, S. Ghanaati, Expansion of the peri-implant attached gingiva with a three-dimensional collagen matrix in head and neck cancer patients-results from a prospective clinical and histological study, Clin. Oral Invest. (2016), https://doi.org/10.1007/s00784-016-1868-2.

[39] S. Ghanaati, A. Kovács, M. Barbeck, J. Lorenz, A. Teiler, N. Sadeghi, C. J. Kirkpatrick, R. Sader, Bilayered, non-cross-linked collagen matrix for regeneration of facial defects after skin cancer removal: a new perspective for biomaterial-based tissue reconstruction, J. Cell Commun. Signal. 10 (2016) 3, https://doi.org/10.1007/s12079-015-0313-7.

[40] S. Al-maawi, A. Orlowska, R. Sader, C.J. Kirkpatrick, S. Ghanaati, In vivo cellular reactions to di ff erent biomaterials — Physiological and pathological aspects and their consequences, 2017.

[41] D. Shendi, J. Marzi, W. Linthicum, A.J. Rickards, D.M. Dolivo, S. Keller, M. A. Kauss, Q. Wen, T.C. McDevitt, T. Dominko, K. Schenke-Layland, M.W. Rolle, Hyaluronic acid as a macromolecular crowding agent for production of cell-derived matrices, Acta Biomater. (2019), https://doi.org/10.1016/j.actbio.2019.09.042.

[42] S. Rother, S.A. Samsonov, S. Moeller, M. Schnabelrauch, J. Rademann, J. Blaszkiewicz, S. Köhling, J. Waltenberger, M.T. Pisabarro, D. Scharnweber, V. Hintze, Sulfated hyaluronan alters endothelial cell activation in vitro by controlling the biological activity of the angiogenic factors vascular endothelial growth factor-A and tissue inhibitor of metalloproteinase-3, ACS Appl. Mater. Interfaces 9 (2017) 9539–9550, https://doi.org/10.1021/acsami.7b01300.

[43] L. Koehler, S. Samsonov, S. Rother, S. Vogel, S. Köhling, S. Moeller, M. Schnabelrauch, J. Rademann, U. Hempel, M. Teresa Pisabarro, D. Scharnweber, V. Hintze, Sulfated hyaluronan derivatives modulate TGF-β1:receptor complex formation: possible consequences for TGF-β1 signaling, Sci. Rep. 7 (2017), https://doi.org/10.1038/s41598-017-01264-8.

[44] R.J.F.C. do Amaral, N.M.A. Zayed, E.I. Pascu, B. Cavanagh, C. Hobbs, F. Santarella, C.R. Simpson, C.M. Murphy, R. Sridharan, A. González-Vázquez, B. O'Sullivan, F. J. O'Brien, C.J. Kearney, Functionalising collagen-based scaffolds with platelet-rich plasma for enhanced skin wound healing potential, Front. Bioeng. Biotechnol. 7 (2019), https://doi.org/10.3389/fbioe.2019.00371.

[45] J.M. Anderson, A. Rodriguez, D.T. Chang, Foreign body reaction to biomaterials, Semin. Immunol. 20 (2008) 86–100, https://doi.org/10.1016/j.smim.2007.11.004.

[46] J.A. Jones, M. Dadsetan, T.O. Collier, M. Ebert, K.S. Stokes, R.S. Ward, P.A. Hiltner, J.M. Anderson, Macrophage behavior on surface-modified polyurethanes, J. Biomater. Sci. Polym. Ed. 15 (2004) 567–584.

[47] R. Klopfleisch, Macrophage reaction against biomaterials in the mouse model - phenotypes, functions and markers, Acta Biomater. 43 (2016) 3–13, https://doi.org/10.1016/j.actbio.2016.07.003.

[48] A.K. McNally, J.M. Anderson, Foreign body-type multinucleated giant cell formation is potently induced by alpha-tocopherol and prevented by the diacylglycerol kinase inhibitor R59022, Am. J. Pathol. 163 (2003) 1147–1156. http://www.ncbi.nlm.nih.gov/pubmed/12937156. (Accessed 27 January 2017). accessed.

[49] A.K. McNally, J.M. Anderson, Macrophage Fusion and Multinucleated Giant Cells of Inflammation, 2011, pp. 97–111, https://doi.org/10.1007/978-94-007-0763-4_7.

[50] S. Ghanaati, M. Barbeck, J. Lorenz, S. Stuebinger, O. Seitz, C. Landes, A.F. Kovács, C.J. Kirkpatrick, R. a Sader, Synthetic bone substitute material comparable with xenogeneic material for bone tissue regeneration in oral cancer patients: first and preliminary histological, histomorphometrical and clinical results, Ann. Maxillofac. Surg. 3 (2013) 126–138, https://doi.org/10.4103/2231-0746.119221.

[51] M. Barbeck, J. Lorenz, M.G. Holthaus, N. Raetscho, A. Kubesch, P. Booms, R. Sader, C.J. Kirkpatrick, S. Ghanaati, Porcine dermis and pericardium-based, non-cross-linked materials induce multinucleated giant cells after their in vivo implantation: a physiological reaction? J. Oral Implantol. 41 (2015) e267–e281, https://doi.org/10.1563/aaid-joi-D-14-00155.

[52] S. Ghanaati, C. Orth, R.E. Unger, M. Barbeck, M.J. Webber, A. Motta, C. Migliaresi, C. James Kirkpatrick, Fine-tuning scaffolds for tissue regeneration: effects of formic acid processing on tissue reaction to silk fibroin, J. Tissue Eng. Regen. Med. 4 (2010) 464–472, https://doi.org/10.1002/term.257.

[53] S. Ghanaati, M. Barbeck, R. Detsch, U. Deisinger, U. Hilbig, V. Rausch, R. Sader, R. E. Unger, G. Ziegler, C.J. Kirkpatrick, The chemical composition of synthetic bone substitutes influences tissue reactions in vivo : histological and histomorphometrical analysis of the cellular inflammatory response to hydroxyapatite, beta-tricalcium phosphate and biphasic calcium phosphate ce, Biomed. Mater. 7 (2012), 015005, https://doi.org/10.1088/1748-6041/7/1/015005.

[54] W.G. Brodbeck, M.S. Shive, E. Colton, Y. Nakayama, T. Matsuda, J.M. Anderson, Influence of biomaterial surface chemistry on the apoptosis of adherent cells, J. Biomed. Mater. Res. 55 (2001) 661–668. http://www.ncbi.nlm.nih.gov/pubmed/11288096. (Accessed 21 March 2017). accessed.

[55] A. Miron, S. Rother, L. Huebner, U. Hempel, I. Käppler, S. Moeller, M. Schnabelrauch, D. Scharnweber, V. Hintze, Sulfated hyaluronan influences the formation of artificial extracellular matrices and the adhesion of osteogenic cells, Macromol. Biosci. 14 (2014) 1783–1794, https://doi.org/10.1002/mabi.201400292.

[56] S. Al-Maawi, M. Barbeck, C.H. Vizcaíno, R. Egli, R. Sader, C.J. Kirkpatrick, M. Bohner, S. Ghanaati, Thermal treatment at 500°C significantly reduces the reaction to irregular tricalcium phosphate granules as foreign bodies: an in vivo study, Acta Biomater. (2020), https://doi.org/10.1016/j.actbio.2020.11.034.

[57] J.A. Jones, M. Dadsetan, T.O. Collier, M. Ebert, K.S. Stokes, R.S. Ward, P.A. Hiltner, J.M. Anderson, Macrophage behavior on surface-modified polyurethanes, J. Biomater. Sci. Polym. Ed. 15 (2004) 567–584. http://www.ncbi.nlm.nih.gov/pubmed/15264659. (Accessed 2 February 2017). accessed.

[58] S. Rother, J. Salbach-Hirsch, S. Moeller, T. Seemann, M. Schnabelrauch, L. C. Hofbauer, V. Hintze, D. Scharnweber, Bioinspired collagen/glycosaminoglycan-based cellular microenvironments for tuning osteoclastogenesis, ACS Appl. Mater. Interfaces 7 (2015) 23787–23797, https://doi.org/10.1021/acsami.5b08419.

[59] J.M. Anderson, A. Rodriguez, D.T. Chang, Foreign body reaction to biomaterials, Semin. Immunol. 20 (2008) 86–100, https://doi.org/10.1016/j.smim.2007.11.004.

[60] W.G. Brodbeck, Y. Nakayama, T. Matsuda, E. Colton, N.P. Ziats, J.M. Anderson, Biomaterial surface chemistry dictates adherent monocyte/macrophage cytokine expression in vitro, Cytokine 18 (2002) 311–319. http://www.ncbi.nlm.nih.gov/pubmed/12160519. (Accessed 8 July 2017). accessed.

[61] W.G. Brodbeck, J. Patel, G. Voskerician, E. Christenson, M.S. Shive, Y. Nakayama, T. Matsuda, N.P. Ziats, J.M. Anderson, Biomaterial adherent macrophage apoptosis is increased by hydrophilic and anionic substrates in vivo, Proc. Natl. Acad. Sci. U. S.A. 99 (2002) 10287–10292, https://doi.org/10.1073/pnas.162124199.

[62] H. Petite, I. Rault, A. Huc, P. Menasche, D. Herbage, Use of the acyl azide method for cross-linking collagen-rich tissues such as pericardium, J. Biomed. Mater. Res. 24 (1990) 179–187, https://doi.org/10.1002/jbm.820240205.

[63] D. Rothamel, F. Schwarz, M. Sager, M. Herten, A. Sculean, J. Becker, Biodegradation of differently cross-linked collagen membranes: an experimental study in the rat, Clin. Oral Implants Res. 16 (2005) 369–378, https://doi.org/10.1111/j.1600-0501.2005.01108.x.

[64] Y. Zhang, S. Al-Maawi, X. Wang, R. Sader, C.J. Kirkpatrick, S. Ghanaati, Biomaterial-induced multinucleated giant cells express proinflammatory signaling molecules: a histological study in humans, J. Biomed. Mater. Res. (2018), https://doi.org/10.1002/jbm.a.36594 jbm.a.36594.

[65] X.W. Zhu, N.M. Price, R.H. Gilman, S. Recarvarren, J.S. Friedland, Multinucleate giant cells release functionally unopposed matrix metalloproteinase-9 in vitro and in vivo, J. Infect. Dis. 196 (2007) 1076–1079, https://doi.org/10.1086/521030.

[66] S. MacLauchlan, E.A. Skokos, N. Meznarich, D.H. Zhu, S. Raoof, J.M. Shipley, R. M. Senior, P. Bornstein, T.R. Kyriakides, Macrophage fusion, giant cell formation, and the foreign body response require matrix metalloproteinase 9, J. Leukoc. Biol. 85 (2009) 617–626, https://doi.org/10.1189/jlb.1008588.

[67] M. Du, Y. Wang, Z. Liu, L. Wang, Z. Cao, C. Zhang, Y. Hao, H. He, Effects of IL-1β on MMP-9 expression in cementoblast-derived cell line and MMP-mediated degradation of type I collagen, Inflammation 42 (2019) 413–425, https://doi.org/10.1007/s10753-018-00951-6.